Variable line-space gratings: new designs for use in grazing incidence spectrometers

Michael C. Hettrick and Stuart Bowyer

Applied Optics Vol. 22, Issue 24, pp. 3921-3924 (1983)

http://dx.doi.org/10.1364/AO.22.003921

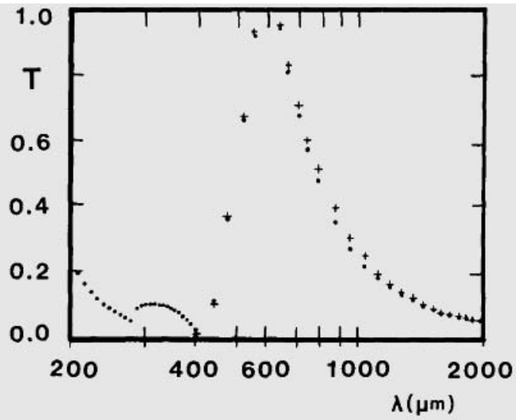

Fig. 4. Normal-incidence transmittance calculated as a function of wavelength for meshes with $a/g = 0.075$, $b/g = 0.14$, and $g = 410\ \mu$m. Points ● correspond to $h/g = 0.016$, while points + correspond to $h/g = 0.0016$.

other experimental curves of Ref. 3 and our theoretical curves.

The good agreement between theory and experiment in Figs. 2 and 3 demonstrates that our formulation provides a reliable basis for the design of meshes with cross-shaped apertures for use in bandpass filters.

R. C. McPhedran acknowledges financial support provided by His Royal Highness Prince Nawaf Bin Abdul Aziz of the Kingdom of Saudi Arabia through the Science Foundation for Physics within the University of Sydney.

References

1. J. E. Davis, Infrared Phys. **20**, 287 (1980).
2. V. P. Tomaselli, D. C. Edewaard, P. Gillan, and K. D. Moller, Appl. Opt. **20**, 1361 (1981).
3. S. T. Chase and R. D. Joseph, Appl. Opt. **22**, 1775 (1983).
4. R. C. Compton, R. C. McPhedran, G. H. Derrick, and L. C. Botten, Infrared Phys., to appear **xx**, 000 (198x).
5. R. C. McPhedran, G. H. Derrick, and L. C. Botten, in *Electromagnetic Theory of Gratings* (Springer, Berlin, 1980).
6. F. L. Lin, IEEE Trans. Microwave Theory Tech. **MTT-25**, 756 (1977).

Variable line-space gratings: new designs for use in grazing incidence spectrometers

Michael C. Hettrick and Stuart Bowyer

University of California, Space Sciences Laboratory, Berkeley CA 94720

Received 11 August 1983.
Sponsored by W. R. Hunter, Naval Research Laboratory.
0003-6935/83/243921-04$01.00/0.

Spectroscopy is one of the fundamental techniques in astronomy. However, spectroscopic study of sources emitting in the extreme UV (λ ~ 100–1000 Å) and the soft x ray (λ ~ 10–100 Å) is still in its infancy, in part due to a lack of spectrometer designs suited specifically for grazing incidence optics. We introduce two such designs and variations, which have emerged from a study[1] of spectrometer options for the Extreme Ultraviolet Explorer (EUVE) satellite.[2]

Both designs achieve spectral imaging through a smooth variation in the line spacing across a reflection grating. Although variable line-space gratings at grazing incidence have recently been proposed for monochromators[3] and also demonstrated for laboratory spectrometers,[4] our approach is fundamentally different: (1) the gratings are flat, and (2) they are placed to intercept the converging beam from a collecting mirror rather than the diverging beam from a slit. This results in (a) small aberrations over a wide instantaneous range in wavelength, (b) a modest required variation in line spacing across the ruled width, (c) a simultaneous minimization of both the spectral and image height aberrations, and (d) a completely stigmatic zero order image. The slitless arrangement common to our designs is very compact, having no additional length behind the focal plane of the collecting mirror.

A schematic layout of the first design is shown in Fig. 1(a). The grating is mounted in-plane, and a cross section of the converging beam is shown in the dispersion plane. The simplest solution for the line-space variation, and the one adopted for use on EUVE, is shown in Fig. 1(b). It consists of straight grooves whose spacing $d(x)$ is varied by a mechanical ruling machine[5] according to the equation

$$d(x) = m\lambda_0/[\cos\beta(x) - \cos\alpha(x)], \qquad (1)$$

where m is the spectral order, λ_0 is the correction wavelength, and $\alpha(x)$ and $\beta(x)$ are the local graze angles of incidence and diffraction. In the limit of small angles α and β, an approximate estimate to the required variation in line spacing is given by $d(x_{\min})/d(x_{\max}) \simeq (\alpha_{\max}/\alpha_{\min})^2$. This variation is modest due to use of a converging incident beam. Equation (1) is simply the local grating equation. The same result for $d(x)$ has also been obtained through direct use of the light-path function.

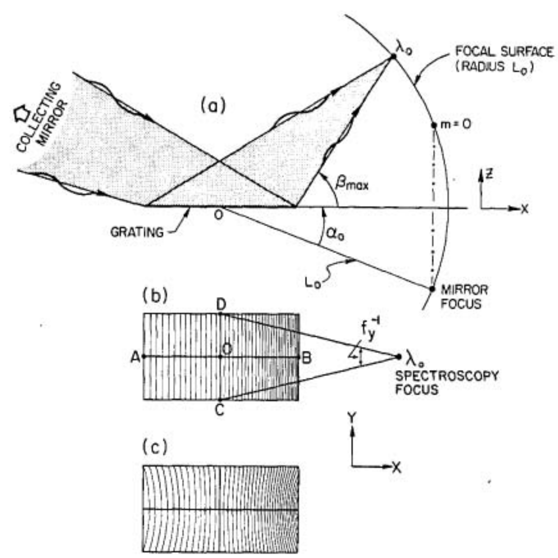

Fig. 1. Geometry of variable line-space plane grating spectrometer. Collecting mirror is upstream of the converging beam: (a) projection upon the dispersion plane; (b) grating plane having variably spaced straight grooves; (c) variably spaced curved grooves, provided by holographic fabrication.

All rays λ_0 illuminating the grating along line AB [Fig. 1(b)] are thereby brought to a point focus, whose distance from grating midpoint O is set equal to the distance L_0 from that midpoint to the mirror focus. All rays λ_0 illuminating groove CD thereby have the same path length difference and, therefore, are also brought to this point focus.

Focal plane aberrations at λ_0 will result from other regions of the grating aperture. The error in the light-path function is

$$\Delta = (m\lambda_0/d_0)[{}^1\!/_2 xy^2 + {}^3\!/_4 x^2y^2(\cos\beta_0 + \cos\alpha_0) - {}^3\!/_8 xy^4 + \ldots], \quad (2)$$

where x and y refer to the coordinate system of Fig. 1 with origin at point O and all distances in units of L_0. Note that there is neither astigmatism nor first-type (tangential) coma, the lowest-order terms being second-type (sagittal) coma and spherical aberration. Converting this wavefront error to image aberrations at the focal plane, we find the resolving power $\lambda/\Delta\lambda \simeq 8f_y^2$ and the image height $H \simeq (L_0/2)(m\lambda_0/d_0)(\alpha_{max} - \alpha_{min})/\alpha_{max}/f_y$, where f_y is the effective focal ratio of the illuminating beam in the y direction.

If this resolution is to be attained, the grating dispersion must overcome any angular uncertainty $(F\epsilon/L_0)$ incident to the grating, where ϵ is the image quality (in seconds of arc) of the collecting mirror, which has focal length F. At the focal plane, this uncertainty is converted into a wavelength blur:

$$[\Delta\lambda]_{dispersive} = 5 \times 10^{-6}(d\lambda/ds)F\epsilon\,(\sin\alpha/\sin\beta), \quad (3)$$

where $(d\lambda/ds)$ is the plate scale. Use of negative (or *inside*) spectral orders, for which $\sin\alpha < \sin\beta$, thus minimizes the wavelength aberrations due to finite ϵ, for a given plate scale. The ratio $(\sin\alpha/\sin\beta)$, or its reciprocal, is also equal to the peak diffraction efficiency of a blazed grating. We find the inside spectral orders to provide for higher diffraction efficiency (and a broad range) at a given spectral resolution, becoming an increasingly significant effect at higher dispersion. At normal incidence, for which $\sin\alpha \simeq \sin\beta \simeq 1$, such differences between $m > 0$ and $m < 0$ are usually not apparent. Adjusting the dispersion to maintain $\lambda/\Delta\lambda = 8f_y^2$ across the spectrum, we find $H \simeq 2 \times 10^{-5}F\epsilon f_y(\alpha_{max} - \alpha_{min})\lambda_0/\lambda_{min}$.

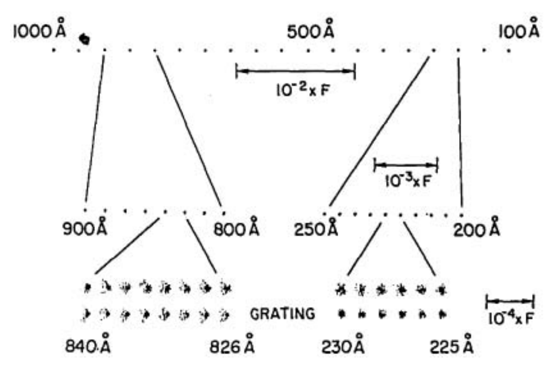

Fig. 2. Ray trace of variable line-space grating illustrated in Fig. 1(b), with straight grooves and a flat detector. System parameters are those given in the text. A resolving power of 700–1100 is achieved simultaneously from 100 to 1000 Å. Lowest spot diagrams show only the grating aberrations.

Figure 2 shows a ray trace of the grating with an $f/5$, $\epsilon = 1$ grazing mirror, and a flat detector. For this example, the grating was placed to intercept $1/6$ of the beam at a distance $L_0 = f/5$ from focus. Thus $(\alpha_{max} - \alpha_{min}) \simeq 1/20$ and $f_y \simeq 10$, leading to predicted grating aberrations of $H \simeq 4 \times 10^{-5}$F and $\lambda/\Delta\lambda \simeq 800$. The actual ray trace, including mirror blur, shows $H \simeq 2 \times 10^{-5}$F and $\lambda/\Delta\lambda = 700$–$1100$. These results are slightly better than predicted, due to the grating aperture being underilluminated by the (annular) mirror beam.

Apparent in Fig. 2 is that the instantaneous spectral coverage is potentially very large (100–1000 Å). This results because the $\lambda = 0$ $(m = 0)$ image is stigmatic, resulting in nearly equal plate scales at λ_0 from all points on the grating aperture. Thus aberrations cannot grow rapidly away from λ_0, leading to wide spectral coverage. For ease of calculation, a cylindrical detector of radius L_0 was centered at point O on the grating, so as to pass through both the stigmatic point $m = 0$ and the correction wavelength λ_0. This choice minimizes all image heights and leads to the spectral range

$$\lambda_{max}/\lambda_{min} \simeq 1 + c \times 10^5(\lambda/\Delta\lambda)^{-2}(F\epsilon/L_0)^{-1}(\alpha_{max} - \alpha_{min})^{-1}, \quad (4)$$

where $\lambda/\Delta\lambda$ is maintained across the entire range λ_{min} to λ_{max}. For the chosen focal surface, $c = 4$. This equation underes-

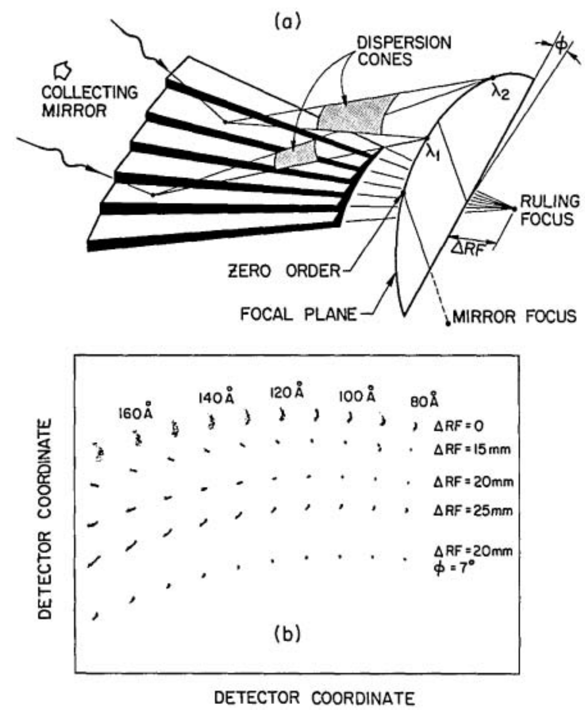

Fig. 3. Oriental fan grating in conical diffraction. Grooves are spaced equally per polar angle about a vertical line through the ruling focus, located behind the focal plane: (a) perspective drawing showing the diffraction cones and the blazed groove profiles; (b) five ray traces showing the effect of various displacements of the ruling focus (ΔRF). Bottom ray trace shows the improvement obtained by tilting the detector. System parameters are those given in text. Only the grating aberrations are shown.

timates that achievable with even a flat detector optimally oriented to minimize wavelength aberrations rather than image heights. For example, it predicts $\lambda_{max}/\lambda_{min} \simeq 4$ for the system ray traced in Fig. 2, which shows $\lambda_{max}/\lambda_{min} = 10$. Of course, in a practical spectrometer the wavelength range is also limited by filter bandpasses and by the curve of diffraction efficiency.

The use of a plane grating results in a stigmatic image at $m = 0$. This is the key to use of photoresist (holographic) methods[6] to improve the above design by generating a completely stigmatic image at λ_0. Two coherent light sources of wavelength λ_0 will produce standing waves, for which the light paths differ by an integral number of wavelengths. The interference patterns are hyperboloids of revolution about the axis joining the two source points. Consider these sources to be placed at the focal positions of $\lambda = \lambda_0$ and $m = 0$ and employ a flat substrate coated with photoresist. The resulting interference fringes become curved grating grooves [Fig. 1(c)], which, when illuminated by a beam having the assumed focus, produce aberration-free (stigmatic) images at $\lambda = \lambda_0$ and $m = 0$. The fabrication method can use coherent light of wavelength λ_0 or possibly de Broglie waves from low-energy electrons of wavelength λ_0, or conventional UV lasers on an enlarged photoresist subsequently reduced to form the grating mask. The latter scaling process is made possible by the flat grating surface.

For the special case in which the line joining the two sources is perpendicular to the grating plane, the grooves in this plane are concentric circles centered at the point of intersection, and the focal surface is the line joining those sources [extension of the dot–dash line in Fig. 1(a)]. This groove geometry has the unique property that all rays hitting any one groove come to the same point focus, as the path length difference is constant, and this holds for all wavelengths. All image heights thereby vanish, and wavelength aberrations away from λ_0 are given by Eq. (4) with $c = 2$. Even for the source geometry of Fig. 1(a), circular grooves with varying curvature are found to remove both the comatic and spherical terms in Eq. (2), leaving a residual aberration $\lambda/\Delta\lambda \simeq (128/3)f_y^4$. Given the system parameters used above, the grating aberration limit to $\lambda/\Delta\lambda$ rises from 800 to 4×10^5 and is 27,000 if ½ rather than ⅙ of the beam is accepted by the grating. Particularly for the special case which leads to concentric grooves and complete stigmatism at λ_0, the required curved grooves represent a simple motion for a mechanical ruling machine. The resulting blazed grating can function as an echelle. Alternately, straight grooves could provide the above correction at λ_0 if ruled on a nonspherical surface whose curvature is small but follows the patterns indicated for curved grooves.

The fact that holographic recording upon a flat grating surface generates completely stigmatic points at $\lambda = \lambda_0$ and $\lambda = 0$ can be generalized to off-plane gratings and leads us to our second general design. Consider two light sources positioned symmetrically on opposite sides of the in-plane dispersion plane shown in Fig. 1(a). The result is a series of hyperbolic grooves which can be approximated as shown in Fig. 3(b), by straight grooves which radiate from a ruling focus located behind the focal plane. This *oriental fan* geometry is used in conical diffraction[7] and can conceivably be ruled mechanically by a simple motion which rotates the grating sample by equal angles between grooves.

For this extreme off-plane (conical) mount, linear dispersion per unit wavelength is L/d, where L = distance to focus and d = groove spacing. The optimal displacement $(\Delta RF)_{opt}$ of the ruling focus behind the focal plane minimizes the variation of this L/d ratio across the grating aperture:

$$(\Delta RF)_{opt} \simeq L_0 \sin^2\gamma_0 \cos\gamma_0, \tag{5}$$

where L_0 and γ_0 are the values of L and the graze angle at the grating center. The fan grating geometry is thus not specific to a particular mounting, so a single grating can be used over a range of incident graze angles, given the constraint of Eq. (5). With this constraint, straight grooves near the center of the grating are tangent to the hyperbolas from a stigmatic holographic ruling. This choice is confirmed by ray tracing, as shown in Fig. 3(b), where $\lambda_0 = 125$ Å, $f_y = 6.3$, $\gamma_{max} - \gamma_{min} = 1/20$, and $(\Delta RF)_{opt} = 19$ mm. The wavelength spots are elongated, and ±25% shifts in ΔRF about the optimal value serve only to rotate the direction of this elongation slightly out of the dispersion direction.

In general, given the ruling focus displacement of Eq. (5), the aberrant light-path function at λ_0 is

$$\Delta = (m\lambda_0/d_0)[\tfrac{1}{2}x^2y\gamma_0^2 + \tfrac{1}{6}y^3 + \ldots]/\cos^2\gamma_0, \tag{6}$$

where all distances are in units of L_0. The origin is at the geometric center of the grating, and the x axis lies along the central groove ($y = 0$). Since this groove is everywhere equidistant from the focal plane positions of $m = 0$ and $\lambda = \lambda_0$, all rays λ_0 hitting this central groove come to a point focus. Therefore, Eq. (6) has no astigmatic term. Converting the wavefront error Δ to image aberrations at λ_0, we find an image height $H/L_0 \simeq (\tfrac{1}{2}m\lambda_0/d_0)(\gamma_{max} - \gamma_{min})/f_y$ and a spectral resolution $\lambda/\Delta\lambda \simeq 8f_y^2/[1 + f_y^2(\gamma_{max} - \gamma_{min})^2]$. It is apparent in Fig. 3(b) that aberrations in $\lambda/\Delta\lambda$ grow rapidly longward of λ_0. These can be minimized by a tilt ϕ of the focal plane, as defined in Fig. 3(a), resulting in the bottom raytrace of Fig. 3(b).

Each of the above two grating designs (in-plane and conical fan), and variations having curved grooves, can be used alone. However, Eq. (4) indicates the spectral coverage to narrow rapidly with increases in resolving power. Using the mirror parameters given above, a $\lambda/\Delta\lambda = 10^4$ leads to a spectral coverage $(\lambda_{max} - \lambda_{min})/\lambda_{min}$ of only ~1% for the in-plane grating design. Fortunately, two variable line-space gratings can be mounted in series, allowing the second grating to separate overlapping echelle orders produced by the first grating. Such an echelle spectrometer covers a wide spectral range at high resolution.

The construction of an echelle spectrometer from these gratings is made possible because the first grating produces a continuum of foci (the dispersed wavelengths), each of which the second grating treats as an (off-axis) mirror focus. Figure 4 shows one possible combination, where highly dispersed wavelengths off an in-plane echelle enter a conical cross-disperser. (Alternatively, the conical cross-disperser may precede the in-plane echelle, thereby minimizing the spread of graze angles into the second grating.) The cross-disperser aberrations are minimized at the wavelengths off the echelle for which the focal plane is displaced from the (fixed) ruling focus of the cross-disperser by $(\Delta RF)_{opt}$, as given by Eq. (5). Given a focal surface which minimizes echelle aberrations and given reasonable values of dispersion, the displacement error $\Delta RF - (\Delta RF)_{opt}$ at the extreme edges of the spectrum is found to be within the accuracy in determination of $(\Delta RF)_{opt}$. The latter results from the range in $L \sin^2\gamma \cos\gamma$ across the grating and was approximately ±25% for the system ray traced in Fig. 3(b). Thus the focal surface for the cross-disperser coincides with that of an echelle, resulting in a 2-D echellogram focused upon the detector. This allows a large range in wavelength to be covered instantaneously at the high spectral resolution delivered by the echelle.

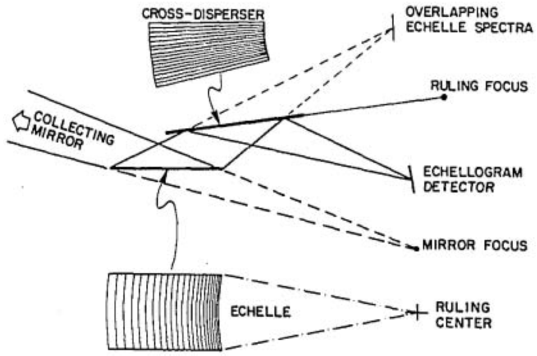

Fig. 4. Two-element echelle spectrometer consisting of two variable line-space gratings. First grating is mounted in-plane and has concentric circularly ruled grooves. Second grating is mounted in conical diffraction with radially ruled grooves from a ruling focus.

As an echelle, the in-plane grating requires a variable blaze angle to maintain blazing in the high orders. The fan grating has a nearly uniform blaze, varying by only a fraction $\sim (\gamma_{max} - \gamma_{min})\gamma_0/2$ across its aperture, but as an echelle requires curved grooves. Thus a second possible combination is to follow a cross-disperser in-plane grating by a conical echelle having curved grooves. Other variations include the use of one grating design (in-plane or conical) for both the echelle and the cross-disperser.

Finally, we note that any of the above designs, including single gratings, can be transformed into a slit spectrometer by use of a relay optic.[8] This optic can also slow the beam convergence, reducing the grating aberrations.

To summarize: we have introduced two new classes of grazing incidence gratings and several variations, which can be used individually or in combination; and have illustrated one combination in the form of an echelle spectrometer. These designs represent ideal candidates for moderate to high resolution spectrometers on such missions as the Far Ultraviolet Spectroscopic Explorer (FUSE, now *Columbus*)[9] and the Advanced X-Ray Astrophysics Facility (AXAF).[10]

We thank C. Martin, P. Jelinsky, and R. Malina for helpful discussions. This work was supported by NASA contract NASW-3636 and NSF grant INT-8116729. Stuart Bowyer is also with the University of California at Berkeley, Astronomy Department.

References

1. M. C. Hettrick, MCH/EUVE/321/82, U. California (Berkeley, 1982).
2. S. Bowyer, R. Malina, M. Lampton, D. Finley, F. Paresce, and G. Penegor, Proc. Soc. Photo-Opt. Instrum. Eng. **279,** 176 (1981).
3. D. E. Aspnes, J. Opt. Soc. Am. **72,** 8 (1982).
4. T. Kita, T. Harada, N. Nakano, and H. Kuroda, Appl. Opt. **22,** 512 (1983).
5. T. Harada and T. Kita, Appl. Opt. **19,** 3987 (1980).
6. J. M. Lerner, Proc. Soc. Photo-Opt. Instrum. Eng. **240,** 82 (1980).
7. M. Neviere, D. Maystre, and W. R. Hunter, J. Opt. Soc. Am. **68** 1106 (1978).
8. R. C. Chase, A. S. Krieger, and J. H. Underwood, Appl. Opt. **21,** 4446 (1982).
9. Final Report of the Science Working Group for the Far Ultraviolet Spectroscopic Explorer, NASA headquarters publication (Apr. 1983).
10. G. W. Clark, Phys. Today **35,** No. 11, 26 (1982).

A REMINDER

Authors submitting Rapid Communications for publication must remember to include a letter from their institution agreeing to honor the publication charge. Otherwise publication will be delayed—and the whole idea of this section of Letters to the Editor is defeated.